

Photon emission in QGP using AdS/QCD at finite chemical potential

M. A. Martin Contreras*, J. M. R. Roldan Giraldo†

High Energy Group, Department of Physics, Universidad de los Andes

Abstract

We calculate the photon emission rate and the electrical conductivity of the QGP at finite temperature and finite chemical potential using AdS/QCD approximations in an AdS Reissner Nordstrom background. To do so, we supposed the medium properties to be encoded in a geometric background. The results obtained in the hard wall and soft wall model are consistent with the observed phenomenology and they also in agree with other holographic results, as the D3/D7 or the Sakai Sugimoto models, suggesting the universality of AdS/CFT conjecture as tool to explore QCD.

1 Introduction

In its beginnings, string theory was expected to be a possible model for strong interactions. But it was eclipsed by the greatest QCD outcomes, making it to be forgotten as fundamental theory for such interactions. Nowadays, with the development of the so-called gravity/gauge duality, string theory recovers its original motivation becoming a tool to explore the strong interactions at their non-perturbative region even at extreme scenarios with finite temperature and chemical potential. These scenarios are observed at nuclei accelerators and stars center. Duality itself suggests that gravitational dual of QCD should exist. The real problem is how to find it.

In this direction, the most successful approximation to gravity/gauge duality is the AdS/CFT Correspondence by J. Maldacena [1], which has been used as a tool to describe non-perturbative hadronic phenomena, specially the quark gluon plasma observed in heavy ion collisions. Properties such as the entropy density, bulk viscosity, jet quenching, photon/dilepton emission rate were well described holographically in the zero chemical limit by top/down approaches as the Dp/Dq system [2] or the Sakai Sugimoto model [3]. Also the bottom/up realizations as the improved holographic QCD model [4] have described the QGP system. Recently, [5] have discussed the shear viscosity and photon emission in the QGP in the latter model. In the AdS/QCD realm, some approximations have been made in the references [6] where they calculated the spectral density for photons in a specific gravitational setup using the soft wall model. Also [7] has calculations for the hard wall

*ma.martin41@uniandes.edu.co

†jroldan@uniandes.edu.co

and the soft wall model for finite chemical potential modeled by the probe D-brane method, in which the DBI action is minimized in order to obtain the embedding profile generated by a U(1) static field. A good review of the holographic approximation to the QGP phenomenology is [8].

This paper is organized as follows: in section 1 we discuss the photon emission rate and the conductivity from the quantum field theory side. In section 2, we set the general background for both hard wall and soft wall models. In section 4 it is discussed how we calculate the trace of the spectral function analytically for each AdS/QCD model. In section 5, we consider the numerical results obtained for the photon emission rate and the conductivity. Finally in section 6 we enunciate the conclusions for our work.

2 Photon Emission Rate

It is well known that any thermal medium composed of charged particles will radiate photons. This photon spectrum can be used as a probe to study the characteristics of such thermal medium, since it depends on its specific properties.

In the case of the QGP produced in heavy ion collisions, the thermal medium is optically transparent due to the small spatial extension¹ and the smallness of electromagnetic coupling. Therefore, any emitted photon escapes from the plasma ball without any further interaction with the medium. In such a situation the spectrum can be considered as *almost planckian*, but it is still useful to obtain information about the plasma in the emission point.

At this point a remark must be done: depending on the momentum k of the emitted photons the dynamics can be split in specific regimes defined by three characteristic length scales, the hard, soft and ultra-soft scales [9].

The hard scale is defined when the limit $k \approx T$ is reached. Contributions of excitations in this scale dominate the bulk thermodynamic properties such as total momentum density and total energy of the plasma, likewise conserved charge susceptibilities. These excitations also control the transport properties in the colored medium.

The second scale, soft scale, is reached when $k \approx gT$, where g is the gauge theory coupling. In this scenario the Landau damping and also the Debye screening, due principally to the coherent interaction of the particles in the thermal colored medium, become important. These effects are treated with the hard-thermal-loop perturbation theory [10, 11, 12, 13].

The third scale is the ultrasoft or non-perturbative: $k \approx g^2T$. In this scale, low frequency and long wave-length dynamics gives the hydrodynamical regime. Photons produced in this regime carry information about properties such as the electrical conductivity. Soft and hard photons produced in more energetic scenarios tends to be suppressed due to the Landau Pomeranchuk Midgal effect. Photon production in a colored medium was discussed in detail both from strong and weak coupling point of view in reference [14].

Let us consider a QGP defined by a colored quantum system in equilibrium that can be described by a thermal field theory in the strongly coupling limit. It will be assumed that the electromagnetic interaction between matter and photons is given by the minimal coupling of a photon field with the electromagnetic current, $e A^\mu J_\mu^{em}$, with e the electromagnetic coupling.

¹At this point, the assumption that the photon mean free path is bigger than the plasma ball size was taken.

At leading order, the photo-production is given by the expression [12]

$$d\Gamma_\gamma = \frac{d^3q}{(2\pi)^3} \frac{e^2}{2(k^0)^2} \eta^{\mu\nu} C_{\mu\nu}^R(k) \Big|_{k^0=|\vec{q}|}, \quad (1)$$

where we have defined the photon 4-momentum as $k^\mu = (k^0, \vec{q})$, $\eta_{\mu\nu}$ denotes the Minkowski metric and $C_{\mu\nu}^R(k)$ is the Wightman function defined for electromagnetic currents as,

$$C_{\mu\nu}^R(k) = \int d^4x e^{-ikx} \langle J_\mu^{EM}(0) J_\nu^{EM}(x) \rangle. \quad (2)$$

Notice that the expectation value in (2) is taken in the thermal equilibrium state and $x^\mu = (x^0, \vec{x})$. In the thermal equilibrium limit the Wightman correlator can be written in terms of the spectral density,

$$C_{\mu\nu}^R = n_B(k^0) \chi_{\mu\nu}(k), \quad (3)$$

$$\chi_{\mu\nu} = -2 \text{Im} G_{\mu\nu}^R(k), \quad (4)$$

with n_B the Bose-Einstein distribution and G^R the thermal retarded Green function. At non zero temperature, Lorentz invariance is explicitly broken leaving us a residual rotational symmetry that allows, together with the gauge invariance, to split the thermal Green function into longitudinal and transversal parts.

Since the idea is to model real photon production (implying $k^0 = |\vec{q}|$), it is possible to ignore the longitudinal part and focus on the transversal one only. Then, the trace of the spectral function (4) is written as

$$\chi_\mu^\mu(k) = -4 \text{Im} \Pi^T(k), \quad (5)$$

where Π^T is the transversal part of the spectral density. Keeping in mind all these definitions and results, the photon emission rate is given by

$$\frac{d\Gamma_\gamma}{d^3|\vec{q}|} = \frac{e^2}{(2\pi)^3 2|\vec{q}|} n_B(k^0) \chi_\mu^\mu(k) \Big|_{k^0=|\vec{q}|}. \quad (6)$$

The electrical AC and DC conductivities of the medium are also determined by the trace of the spectral function. From the Kubo formula the AC $\sigma(k^0)$ conductivity can be read from the spatial components of $\chi_{\mu\nu}$ as

$$\sigma_{AC}(k^0) = -\frac{\chi_{ii}(k^0, \vec{k}=0)}{2ik^0}. \quad (7)$$

From the spectral density in the limit of $k_0 \rightarrow 0$ we can read the DC conductivity as

$$\sigma_{DC} = \frac{\alpha_{em}\pi}{2T} \frac{d\chi_\mu^\mu(k^0)}{dk^0} \Big|_{k^0=0}. \quad (8)$$

Then the problem of calculating the photon emission rate and the conductivity translates into the calculation of the trace of the spectral function holographically. This procedure will be realized in the next sections.

3 Holographic Setup

3.1 Geometric Background

We will focus on the calculation of the 2-point function using two of the AdS/QCD models: the hard wall [15, 16] and the soft wall [17] models. These two approximations can be summarized into a single expression just by considering the behavior of a static dilaton Φ field.

In both AdS/QCD models the background is considered dual to the colored medium properties, composed by massless quarks. Since we are considering the finite chemical potential case, it is possible to introduce a charge in the AdS background through an Einstein–Hilbert–Maxwell action. Holographically, we will say that this charge is dual to the generator of the $U(1)$ baryonic symmetry. Following these ideas the background action can be written as

$$I_{\text{Background}} = \frac{1}{16\pi G_5} \int d^5x \sqrt{-g} e^{-\Phi} \left(R - 2\Lambda - \frac{1}{4g_5^2} G_{mn} G^{mn} \right), \quad (9)$$

where $G_{mn} := \partial_m V_n(z, x^\mu) - \partial_n V_m(z, x^\mu)$, the cosmological constant is $\Lambda = -\frac{6}{L^2}$, with L the AdS radius, G_5 is the Newton constant in five dimensions, and the five dimensional gauge coupling is defined as $\frac{1}{g_5^2} = \frac{N_c N_f}{4\pi}$, with N_c and N_f the number of colors and flavors respectively. Adding temperature to a given system holographically means the presence of a black hole, so it is possible to conclude that the minimal coupled Hilbert–Einstein–Maxwell action (9) leads to a the Reissner–Nordstrom AdS Black Hole solution. In other words, this RN AdS BH solution can be considered as the gravitational dual for a strongly coupled plasma under finite chemical potential and finite temperature conditions [18]. Following these ideas, the background is written as:

$$dS^2 = \frac{L^2}{R^2} \left[-h(z) dt^2 + d\vec{x}^2 + \frac{dz^2}{h(z)} \right], \quad (10)$$

where the blackening factor $h(z)$ is fixed by the 1-form potential V_m . If a static solution is chosen, $V_m = -V(z) dt$, the h factor can be written as

$$h(z) = 1 - (1 + q^2 z_h^6) \left(\frac{z}{z_h} \right)^4 + q^2 z_h^6 \left(\frac{z}{z_h} \right)^6, \quad (11)$$

where q is the charge of the black hole and z_h is the event horizon. The temperature is defined using the Hawking–Page relation [19, 20]

$$T = \frac{|h'(z_h)|}{4\pi} = \frac{1}{\pi z_h} \left(1 - \frac{q^2 z_h^6}{2} \right). \quad (12)$$

In pure AdS, i.e. without dilaton, the 1-form potential is given by $V(z) = \mu - q^3 z_h^3 z^2$. In AdS/QCD models the same form cannot be granted due to the presence of the cutoff². In that case it is possible to approximate the AdS/QCD solution to the pure AdS one in the limit $z \rightarrow 0$ [21]. Holographically, the chemical potential μ related to the gauge theory in the boundary is defined in the limit $z \rightarrow 0$ where the 1-form static potential is $V(0) = \mu$.

3.2 Holographic Photons

The QGP will be modeled using a 5-dimensional $U(1)$ field A_m coupled to the static dilaton in the AdS/QCD standard form

$$I_\gamma = -\frac{1}{4g_\gamma^2} \int d^4x \sqrt{-g} e^{-\Phi(z)} F_{mn} F^{mn}, \quad (13)$$

where g_γ^2 is the coupling constant for photons in the QGP, that in general depends on temperature [22, 6] and $F_{mn} = \partial_m A_n - \partial_n A_m$. From the photon action it is possible to obtain the equations of motion for the vector field A_m . To do this, the photons will be supposed to be moving in the x_3 Euclidean direction, then the photon 4-momentum can be fixed to be $k_\mu = (k_0, 0, 0, k_0)$. Therefore, using the background (10) the e.o.m. in Fourier space are written as

$$\partial_z \left[\frac{e^{-\Phi(z)}}{z} h(z) \partial_z A(k, z) \right] + \frac{e^{-\Phi(z)}}{z} k_0^2 [1 - h(z)] A(k, z) = 0, \quad (14)$$

where the gauge fixing $A_z = 0$ was implicitly used and $A(q, z)$ is the transversal field component. The longitudinal components, related to the dilepton production are fixed to be zero.

3.3 Thermal Green Function

The retarded Green function G^R can be constructed with the solutions of eqn. (14). In order to do that, the first step is to evaluate the on-shell boundary photon action obtained from (13):

$$I_{\text{On-Shell}}^{\text{Bndry}} = -\frac{L}{2g_\gamma^2} \int d^4k \left[\frac{e^{-\Phi(z)}}{z} h(z) A(z, k) \partial_z A(z, -k) \right]_{z \rightarrow 0}^{z=z_h}. \quad (15)$$

Following the Minkowskian prescription given in [23], the thermal Green function can be obtained from the integrand in the boundary action, evaluated in the event horizon z_h :

$$G^R(k) = \frac{1}{g_\gamma^2} \frac{e^{-\Phi(z)}}{z} h(z) A(z, k) \partial_z A(z, -k) \Big|_{z=z_h}. \quad (16)$$

With this expression, the trace of the spectral function (4) is given by

²The case of the Hard Wall model is similar to pure AdS since the dilaton is fixed to be zero, but the AdS space is sliced. If it is possible to ensure that the sliced part of the geometry lies outside of the RN AdS BH then the 1-form potential is the same as in pure AdS.

$$\chi_\mu^\mu(k) = -4 \frac{e^{-\Phi(z)}}{z} h(z) \operatorname{Im} A(z, k) \partial_z A^*(z, k) \Big|_{z=z_h} \quad (17)$$

The trace of the spectral function is calculated from the action (13) using the static background (10). In the next sections the discussion will be focused in each AdS/QCD approximation, namely, hard wall and soft wall models.

4 AdS/QCD models

4.1 Hard wall model

Hard wall is defined by fixing the dilaton field to be zero, $\Phi(z) = 0$, together with the Dirichlet condition on the transverse fields at some holographic coordinate $z_\Lambda = 1/\Lambda_{QCD}$ taken as a hard cutoff, where Λ_{QCD} is the QCD energy scale. The physical behavior of the hard wall system is equivalent as the square well in quantum mechanics: the presence of the cutoff induces a discrete set of solutions that defines the eigenstates of the system.

The background action in the hard model is then given by

$$dS^2 = \frac{L^2}{R^2} \Theta(z_\Lambda - z) \left[-h(z) dt^2 + d\vec{x}^2 + \frac{dz^2}{h(z)} \right], \quad (18)$$

where $\Theta(z)$ is the usual step function that defines the AdS slice and h is the warp factor defined in the expression (11). The temperature in this case follows from (12).

To obtain the charge in terms of the chemical potential μ it is necessary to solve the equation of motion for $V(z)$ in the AdS slice and then evaluate the Hilbert–Einstein–Maxwell action to construct the grand canonical potential $\Omega(\mu, T)$.

In order to have a regular solution we will impose that $z_\Lambda = z_h$. From the Hilbert–Einstein–Maxwell action evaluated in the hard wall background (18) it is possible write the equation of motion for the electrostatic potential V as:

$$\partial_z \left[\frac{1}{z} \partial_z V(z) \right] = 0, \quad (19)$$

Subjected to the boundary conditions $V(z_\Lambda) = 0$ and $V(0) = \mu$. The solution under these conditions is $V(z) = \mu \left(1 - \frac{z^2}{z_\Lambda^2} \right)$, and after evaluating the on-shell Hilbert–Einstein–Maxwell action, the grand canonical potential is written as [24, 25, 26]:

$$\Omega(\mu, T) = -\frac{\mu^2 \tau}{g_5^2 z_\Lambda^2(T)}, \quad (20)$$

with τ a fixed volume in the usual Euclidian space than can be fixed to be one and z_Λ is a function of T .

From the classical thermodynamic relation

$$q = - \left. \frac{\partial \Omega}{\partial \mu} \right|_T, \quad (21)$$

we find the relation between the baryonic charge and the chemical potential. Then, we obtain:

$$q = \frac{2\mu\tau}{g_5^2 z_\Lambda^2}. \quad (22)$$

Now that the background is fully characterized we can fix our attention on the photon action in the AdS slice in order to obtain the trace of the spectral density χ_μ^μ . The e.o.m. for the photon field in this hard wall scenario is

$$\partial_z \left[\frac{1}{z} h(z) \partial_z A(z) \right] + \frac{k_0^2}{z h(z)} [1 - h(z)] A(z) = 0. \quad (23)$$

To solve this equation, it is necessary to set the incoming boundary condition as the field A approaches to the horizon. To do this, the field A will be written as $A(z, k) = \left(1 - \frac{z}{z_\Lambda}\right)^{-i\omega z_\Lambda/(2-Q^2)} F(k, z)$, where the F function is fixed to be 1 in z_Λ . Following these ideas we are able to write the trace of the spectral density:

$$\chi_\mu^\mu(k^0) = - \frac{4\mathcal{N} k^0 (1 - q^2 z_\Lambda^6/2)}{z_\Lambda |A(0, k_0)|^2} \quad (24)$$

where the coupling constant is defined as $1/g_\gamma^2 = N_c N_f T^2/8\pi^2 \equiv \mathcal{N}$ [13]. This coupling measures the electric degrees of freedom in the plasma and scales with the temperature, since it enhances the photon production as a consequence of growing the plasma ball.

In general, equations like (23) have no analytical solutions since their highly non-linear behavior, so we need to make use of numerical methods in build up the trace of the spectral densit. In order to do this analysis we will define the adimensional frequency $\omega = k^0/2\pi T$ and baryonic density charge $Q = qz_\Lambda^3$. The results for the trace of the spectral function and the photon production are showed in the figure 1.

4.2 Soft wall model

The static background in the soft wall is defined by the dilaton profile $\Phi(z) = \kappa^2 z^2$, where κ is an energy scale of the hadron spectra in a given Regge trajectory. In this case, it is not univocally defined in terms of the temperature and baryonic density. Thus, as a first approximation, the values of $Q = qz_h^3$ will be taken small in order to use the relation $T = 0.4917\kappa^2$ given by [27].

The chemical potential can be obtained from the Hilbert–Einstein–Maxwell action (9) in this background by virtue of the e.o.m.

$$\partial_z \left(\frac{e^{-\kappa^2 z^2}}{z} \partial_z V(z) \right) = 0. \quad (25)$$

With the boundary conditions $V(z) = \mu$ and $V(z_h) = 0$, the solution for the equation above is in the form

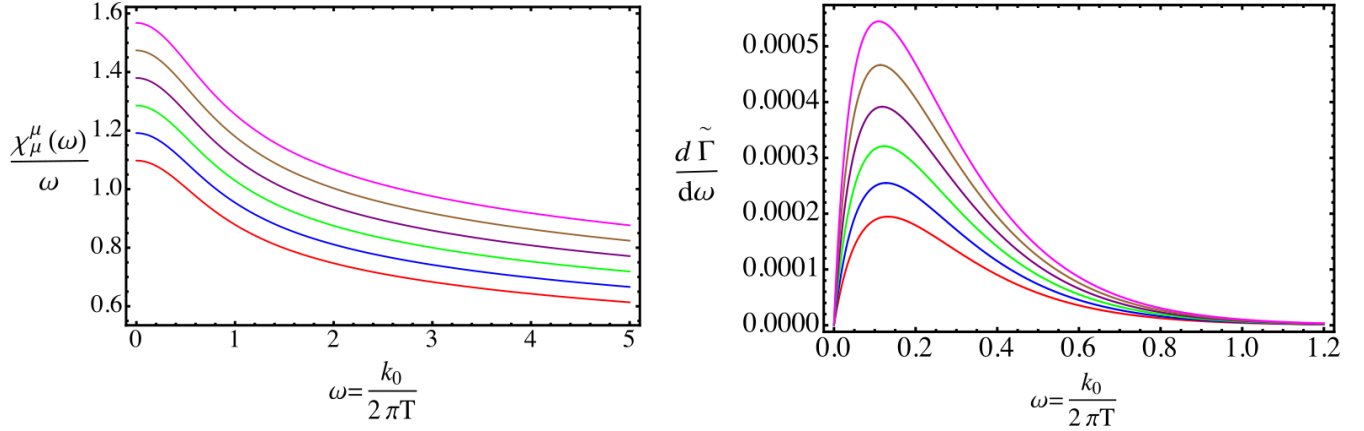


Figure 1: Left panel shows the trace of the normalized spectral function different values of $Q = qz_\Lambda^3$: $Q = 0$ (red), $Q = 0.1$ (blue), $Q = 0.25$ (green), $Q = 0.5$ (purple), $Q = 0.75$ (brown), $Q = 1.0$ (magenta); at the deconfinement temperature for this model given by $T_c = \frac{2^{1/4}}{\pi z_\Lambda} \left(1 - \frac{Q^2}{2}\right)$ in the hard wall model [27]. Right panel shows the normalized (divided by \mathcal{N}) photon emission rate at T_c with the same values of Q .

$$V(z) = \frac{\mu}{1 - e^{\kappa^2 z_h^2}} \left(e^{-\kappa^2 z^2} - e^{-\kappa^2 z_h^2} \right), \quad (26)$$

In order to calculate the baryonic charge we will impose that the 1-form static potential in the limit $z \rightarrow 0$ should match the RN AdS version of it [21]. Evaluating the on-shell Hilbert–Einstein–Maxwell action and using the thermodynamic relation (21) we obtain the baryonic charge as a function of the chemical potential:

$$q = \frac{2L\tau}{g_5^2} \frac{\mu \kappa^2 e^{\kappa^2 z_h^2}}{e^{\kappa^2 z_h^2} - 1}. \quad (27)$$

Once you have fully characterized the background, the next step is the construction of the spectral function starting from the e.o.m in this case

$$\partial_z \left[\frac{e^{-\kappa^2 z^2}}{z} h(z) \partial_z A(z) \right] + \frac{k_0^2 e^{-\kappa^2 z^2}}{z h(z)} [1 - h(z)] A(z) = 0. \quad (28)$$

Imposing the ingoing boundary conditions as in the hard wall case we arrive to the trace of the spectral function given by the expression

$$\chi_\mu^\mu(k^0) = -\frac{4\mathcal{N} k_0 e^{-\kappa^2 z_h^2} (1 - q^2 z_\Lambda^6/2)}{z_\Lambda |A(0, k_0)|^2} \quad (29)$$

with the same \mathcal{N} coupling as in the hard wall is used here. Using the trace of the spectral function it is possible to construct numerically the photon emission rate in terms of Q and ω . The results in this approximation are plotted in the figure 2.

5 Results

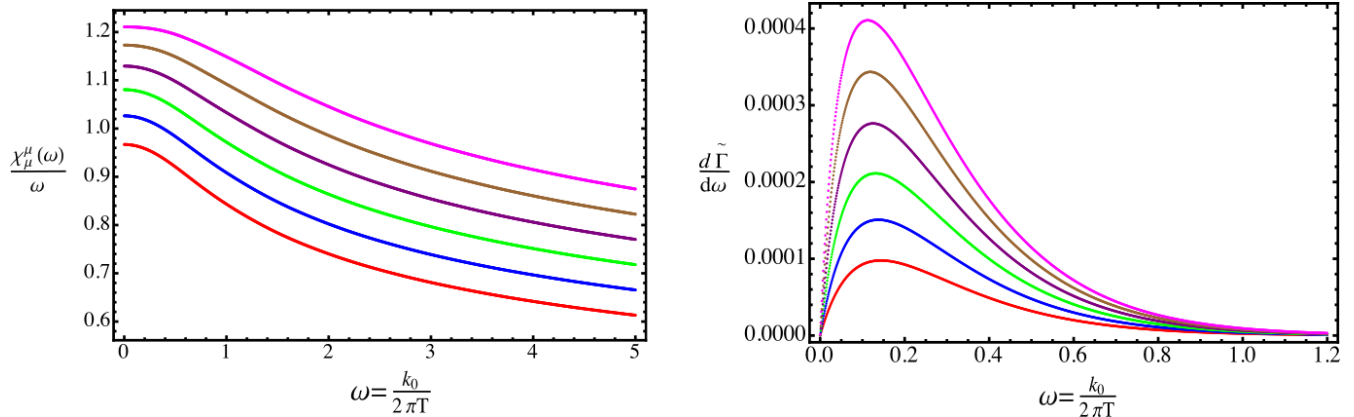


Figure 2: Left panel shows the trace of the normalized spectral function for different values of $Q = qz_\Lambda^3$: $Q = 0$ (red), $Q = 0.001$ (blue), $Q = 0.0025$ (green), $Q = 0.0050$ (purple), $Q = 0.0075$ (brown), $Q = 0.0100$ (magenta); at the deconfinement temperature for this model given by $T_c = 0.4917\kappa^2$ in the soft wall model[27] for small values of Q . Right panel shows the normalized photon emission rate at T_c with the same values of Q .

In order to do the numerical analysis in frequency, the temperature is fixed while the baryonic charge is varying. The results for hard wall and soft wall models are plotted in the figures 1 and 2.

The hard wall model is a holographic bag in the sense that confinement is placed by a hard cutoff fixed by the temperature of the colored medium. Any other extra properties of the medium are hidden in the background. For example, in Dp/Dq systems the quark mass is given by the embedding of the Dq-branes into the Dp-black branes in the decoupling limit [2]. In the case of AdS/QCD models, this specific information can be added with extra fields in the Hilbert–Einstein–Maxwell action. One application of this idea can be seen in [28] where the quark mass is introduced as a scale defined by a bulk mass in a static modified hard wall.

In the case of the soft wall model, the cutoff is a decreasing function of the coordinate z defined by a static dilaton. The energy scale κ is fixed by the temperature of the medium. In other applications of the soft wall model to hadronic spectra the energy scale is fixed by the lightest particle in the spectrum [17]. It is also possible to introduce massive quarks by adding extra fields into the background action. This will be done in future works.

The trace of spectral density on both models behaves monotonically with ω for the explored values of Q . The soft wall model is more sensitive to increasing of Q than the hard wall. This is due to the presence of the dilaton field in the first one. The scale κ is a function of T and Q . For values of Q near to the upper limit, $\sqrt{2}$, the trace of the spectral function is expected to begin to oscillate because the background is unstable for those values of Q [20]. The results for $Q = 0$ are also in agreement with those obtained in [6], where the authors construct a different background in order to simulate the results for the D3/D7 system in the massless quark region and try to study how the trace of the spectral function behaves as a function of κ . Our background and the one showed in that reference differs by the transformation $u = \frac{z^2}{z_h^2}$. It is no surprising that these models

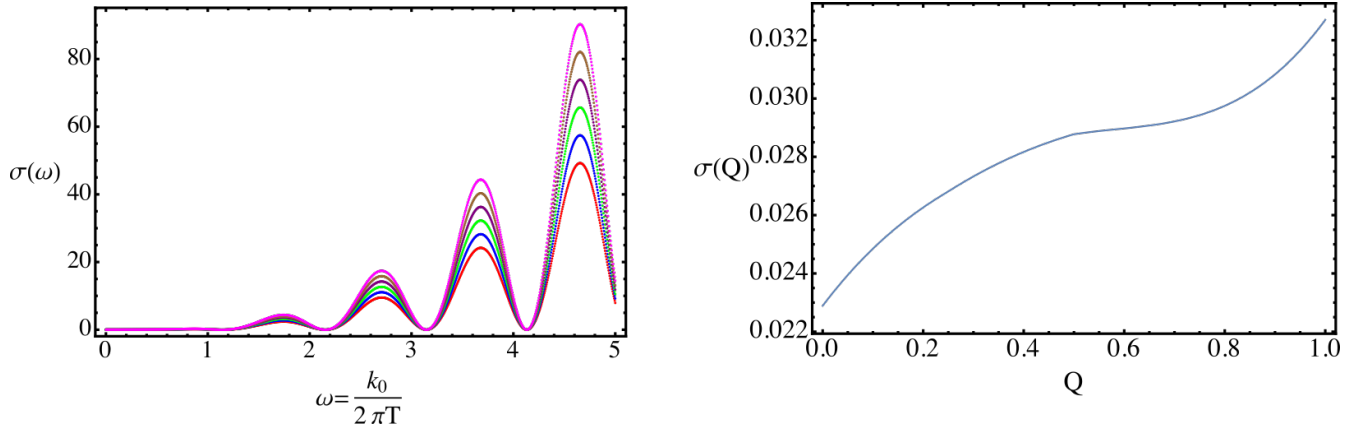


Figure 3: Left panel shows the real part of the AC conductivity calculated with the expression (7) for the hard wall model as a function of the normalized frequency ω for the same values of Q used in figure 1. Right panel shows the DC conductivity calculated from the equation (8) in the hard wall model as a function of the baryonic charge Q .

have similar behaviors. In fact, Dp/Dq systems and AdS/QCD models are AdS-like (or conformal AdS) in the sense of [29].

The photon emission rate obtained for both models (right panels in figures 1 And 2) are also consistent with the QGP phenomenology. The emission occurs for small values of ω , where the ultrasoft behavior is expected [30]. When ω is increased the photon emission is damped, according to the Landau damping effect and Debye screening: photons are reabsorbed by the medium and are suppressed. For high values of ω , the emission goes to zero due to the reduction of bremsstrahlung and pair production, the so called Landau–Pomeranchuk–Migdal effect [31, 32, 33].

When the chemical potential is turned on, the chemical equilibrium is broken, implying that there is an excess in the quark (or anti-quark) population that makes the enhancement of the quark (anti quark) bremsstrahlung over their annihilation radiation, causing that the photon emission rate increases with the chemical potential for low energies [10]. For all the Q values tested, the photon emission rates have common asymptotic behavior with large ω , demonstrating the expected universality in 4+1 strongly coupled plasmas. These results are in agreement with reference [7], where the photon emission rate was calculated starting from the DBI action instead of considering an AdS RN black hole. Holographically, turning on the chemical potential means the phase transition from the AdS Schwarzschild to the AdS RN background.

In the figures 3 and 4 the AC and DC conductivities are plotted. In the hard wall case, the real part of the AC conductivity (left panel in both figures) grows monotonically with ω up to a maximum, then it starts to oscillate. In the case of the soft wall model, the dilaton prevents that the real part of the AC conductivity begins to oscillate, damping the profile. In the case of the DC conductivity (right panels), for both models it is increasing with the baryonic charge for a fixed temperature. This is expected since in the limit $\omega \rightarrow 0$ we are in the ultrasoft limit, where the chemical potential enhances the photon production by the reasons exposed above.

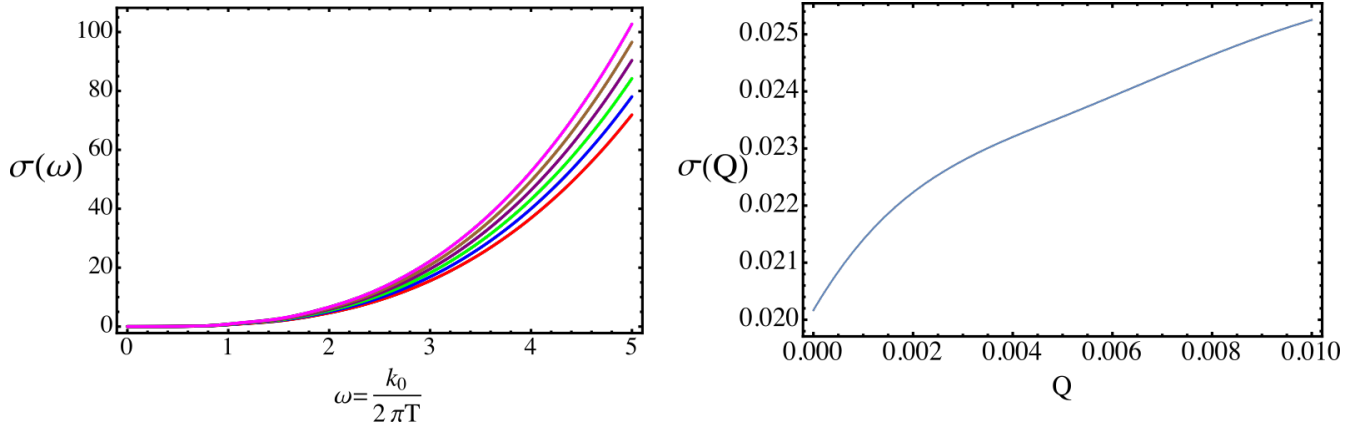


Figure 4: Left panel shows the real part of the AC conductivity calculated with the expression (7) for the soft wall model as a function of the normalized frequency ω for the same values of Q used in figure 2. Right panel shows the DC conductivity calculated from the equation (8) in the soft wall model as a function of the baryonic charge Q .

6 Conclusions

In this work we have discussed the photon emission rate and the conductivity for hard wall and soft wall model under finite chemical potential regime. We have constructed holographically the chemical potential by means of an AdS Reissner–Nordstrom black hole with a static electrical charge. In the perspective of QFT, the holographic procedure showed here is equivalent to consider all the Feynman diagrams allowed by the Landau–Pomeranchuk–Midgal effect that have photons as external legs.

It is also interesting to comment that the results showed here are in agreement with other top/down models used to study photon emission [7, 22] despite the fact that they are constructed in different backgrounds, as in the case of the Sakai Sugimoto discussed in [3]. The evidence that different holographic approaches can model the same phenomenology encodes an underlying nature: gravity can be connected to strong interactions in a deep way that we are just beginning to uncover.

These models are a good approximation to the study of the excited colored matter created in heavy ion collisions. An interesting next step would be the description of these AdS RN solutions for low temperature, in order to study possible applications to nuclear physics.

Acknowledgments: Authors want to thank the Vicedecanatura de Investigaciones of Universidad de los Andes.

References

- [1] J. Maldacena. *Large N field limit of superconformal field theories and supergravity*. Advances in Theoretical and Mathematical Physics, 2 (231), 1998.

- [2] D. Mateos and L. Patiño. *Bright branes for strongly coupled plasmas*. JHEP, 2007(11):025, 2007.
- [3] Y. Y. Bu and J. M. Yang. *Structure functions of holographic quark gluon plasma: Sakai-Sugimoto model versus its non critical version*. Phys. Rev. D, 84:106004, 2011.
- [4] U. Gursoy and E. Kiritsis. *Exploring improved holographic theories for QCD: part I*. JHEP, 2008(02):032, 2008.
- [5] D. L. Yang and B. Muller. *Shear viscosities of photons in strongly coupled plasmas*. Phys. Lett. B, 760:565–570, 2016.
- [6] A. Nata Atmaja and K. Schalm. *Photon and dilepton production in soft wall AdS/QCD*. JHEP, 2010(8):124, 2010.
- [7] Y. Y. Bu. *Photoproduction and conductivity in dense holographic QCD*. Phys. Rev. D, 86:026003, 2012.
- [8] R. A. Janik. *The dynamics of Quark Gluon Plasma and AdS/CFT*, p. 147–181. Springer Berlin, 2011.
- [9] E. Shuryak. *The QCD vacuum, Hadrons and Superdense Matter*, volume 71, World Scientific Lecture Notes in Physics. World Scientific, 2014.
- [10] S. Somorendro Singh. *Free energy and direct photon emission at finite chemical potential*. Journal of Physics: Conference series, 535(1):012002, 2014.
- [11] H. Gervais and S. Jeon. *Photon production from a quark gluon plasma at baryon chemical potential*. Phys. Rev. C, 86:034904, 2012.
- [12] P. Arnold, G. D. Moore and L. G. Yaffe. *Photon emission from ultrarelativistic plasmas*. JHEP, 2001(11):057, 2001.
- [13] P. Arnold, G. D. Moore and L. G. Yaffe. *Photon emission from quark gluon plasma: complete leading order results*. JHEP, 2001 (12):009, 2001.
- [14] S. C. Simon, P. Kovtun, G. D. Moore. *Photon and dilepton production in supersymmetric Yang–Mills plasma*. JHEP, 2006(12):015, 2006.
- [15] J. Polchinski and M. J. Strassler. *Hard scattering and gauge/string duality* Phys. Rev. Lett., 88:031601, 2002.
- [16] H. Boschi-Filho and N. R. F. Braga. *QCD/String holographic mapping and glueball mass spectrum*. Eur. Phys. J. C, 32(4):529–533, 2004.
- [17] A. Karch, E. Katz, D. T. Son and M. A. Stephanov. *Linear confinement in AdS/QCD*. Phys. Rev. D, 74:015005, 2006.

- [18] K. Jo and S. J. Sin. *Photoemission rate of strongly interacting quark–gluon plasma at finite density*. Phys. Rev. D, 83:026004, 2011.
- [19] S. W. Hawking and H. S. Reall. *Charged and rotating AdS black holes and their CFT duals*. Phys. Rev. D, 61:024014, 1999.
- [20] R. G. Cai and J. P. Shock. *Holographic confinement/deconfinement phase transition of AdS/QCD in curved spaces*. JHEP, 2007(08):095, 2007.
- [21] P. Colangelo, F. Giannuzzi and F. Zuo. *Temperature and chemical potential dependence of the gluon condensate: a holographic study*. Phys. Rev. D, 88:115011, 2013.
- [22] L. Patiño and D. Trancanelli. *Thermal photon production in a strongly coupled anisotropic plasma*. JHEP, 2013(2):154, 2013.
- [23] D. T. Son and A. O. Starinets. *Minkowski–space correlators in AdS/CFT correspondence: recipe and applications*. 2002(09):154, 2013.
- [24] S. Nakamura. *Comments on chemical potentials AdS/CFT*. Progress of Theoretical Physics, 119(5):839–849, 2008.
- [25] Y. Seo and S. J. Sin. *Baryon mass in medium with holographic QCD*. JHEP, 2008(04):010, 2008.
- [26] S. Nakamura, Y. Seo and K. P. Yogendran, *Baryon-charge chemical potential in AdS/CFT*. Progress of Theoretical Physics, 120(1):51–76, 2008.
- [27] C. P. Herzog, *Holographic Prediction for the deconfinement temperature*. Phys. Rev. Lett., 98:091601, 2007.
- [28] N. R. F. Braga, S. Diles and M. A. Martin Contreras. *Holographic model for heavy–vector–meson masses*. EPL (Europhysics Letters), 115(3):31002, 2016.
- [29] I. Kanitscheider, K. Skenderis and M. Taylor. *Precision Holography for non–conformal branes*. JHEP, 2008(09):094, 2008.
- [30] S. Endres, H. van Hees and M. Bleicher. *Photon and dilepton production at the facility for antiproton and ion research and beam-energy scan at the relativistic heavy-ion collider using coarse–grained microscopic transport simulations*. Phys. Rev. C, 93:054901, 2016.
- [31] D. Dutta, K. Kumar, A. K. Mohanty and R. K. Choudhury. *Chemical equilibration and thermal dilepton production from the quark gluon plasma at finite baryon density*. Phys. Rev. C, 60:014905, 1999.
- [32] P. Aurenche, F. Gelis, H. Zaraket and R. Kobes. *Bremsstrahlung and photon production in thermal QCD*. Phys. Rev. D, 58:085003, 1998.
- [33] P. Aurenche, F. Gelis, G. D. Moore and H. Zaraket. *Landau–Pomeranchuk–Midgal resummation for dilepton production*. JHEP, 2002(12):006, 2002.